Climatic variations during the Holocene inferred from radiocarbon and stable carbon isotopes in **speleothems from** a high-alpine cave

Caroline Welte[1,2], Jens Fohlmeister[3,4], Melina Wertnik[1,2], Lukas Wacker[1], Bodo Hattendorf[5], Timothy I. Eglinton[2], Christoph Spötl[6]

[1] Laboratory of Ion Beam Physics, ETHZ, Otto-Stern Weg 5, 8093 Zurich, Switzerland,

[2] Geological Institute, ETHZ, Sonnegstrasse 5, 8092 Zurich, Switzerland

[3] Potsdam Institute for Climate Impact Research, Telegrafenberg, 14473 Potsdam, Germany

[4] GFZ German Research Centre for Geosciences, Section 'Climate Dynamics and Landscape Development', 14473 Potsdam, Germany

[5] Laboratory of Inorganic Chemistry, D-CHAB, ETHZ, Vladimir-Prelog Weg 1, 8093 Zurich, Switzerland

[6] Institute of Geology, University of Innsbruck, Innrain 52f, 6020 Innsbruck, Austria

Keywords: radiocarbon, stable carbon isotopes, LA-AMS, speleothems, high-alpine cave

Correspondence to: Caroline Welte: cwelte@phys.ethz.ch, Jens Fohlmeister: jens.fohlmeister@pik-potsdam.de

Abstract

Rapid and continuous analysis of radiocarbon (^{14}C) concentration in carbonate samples at ~~very high~~ spatial resolution down to 100 μm has been made possible with the new LA-AMS (laser ablation accelerator mass spectrometry) technique. This novel approach can provide radiocarbon data at a spatial resolution similar to that of stable carbon (C) isotope measurements by isotope ratio mass spectrometry ~~(IRMS)~~ of micromilled samples and, thus, can help to interpret δ^{13}C signatures, which otherwise are difficult to understand due to numerous processes contributing to changes in C-isotope ratio. In this work, we analyzed δ^{13}C and ^{14}C on the Holocene stalagmite SPA 127 from the high-alpine Spannagel Cave (Austria). Both proxies respond in a complex manner to climate variability. Combined stable carbon and radiocarbon profiles allow to identify three growth periods characterized by different δ^{13}C signatures: (i) the period 8.5 to 8.0 ka BP is characterized by relatively low δ^{13}C values with small variability combined with a comparably high radiocarbon reservoir effect (expressed as dead carbon fraction, dcf) of around 60%. This points towards C contributions of host rock dissolution and/or from an "old" organic matter (OM) reservoir in the karst potentially mobilized due to the warm climatic conditions of the early Holocene. (ii) Between 8 and 3.8 ka BP a strong variability in δ^{13}C ~~reaching~~ with values ranging from -8 to +1‰ ~~with~~ and a generally lower dcf ~~was observed~~. The δ^{13}C variability is most likely caused by changes in C exchange between cave air CO_2 and dissolved inorganic carbon in drip water ~~gas exchange processes~~ in the cave, which are induced by reduced drip rates as derived from reduced stalagmite growth rates. Additionally, the lower dcf indicates that the OM reservoir contributed less to stalagmite growth in this period possibly as a result of reduced meteoric precipitation or because it was exhausted. (iii) In the youngest section between 3.8 and 2.4 ka BP, comparably stable and low δ^{13}C values combined with an increasing dcf reaching up to 50% again hint towards a contribution of an aged OM reservoir in the karst. This study reveals the ~~high~~ potential of combining high-resolution ^{14}C profiles in speleothems with δ^{13}C records in order to disentangle climate-related C dynamics in karst systems.

1 Introduction

Understanding the climate of the past is the key for understanding how climate and environment will change in the future. Insights into paleoclimate are gained through the study of archives with stalagmites being a prominent example for a terrestrial archive. Stalagmites can grow continuously over thousands to tens of thousands of years (Cheng et al., 2016; Fairchild et al., 2006; Moseley et al., 2020). Caves hosting stalagmites are present on all continents except Antarctica and uranium-series disequilibrium dating allows to build robust chronologies (Cheng et al., 2013; Richards and Dorale, 2003; Scholz and Hoffmann, 2008). Trace-element and stable isotope data of stalagmites allow the reconstruction of climatic conditions in the past. For example, the oxygen isotope composition (δ^{18}O) is generally interpreted as a combination of a temperature and a meteoric precipitation signal (Lachniet, 2009; Wackerbarth et al., 2010). The interpretation of the stable carbon isotope signature (δ^{13}C), however, is more challenging since additional local effects, such as vegetation changes (e.g., Bar-Matthews et al., 1999; Denniston et al., 2007; Fohlmeister et al., 2020), the carbonate dissolution mechanism (e.g., Fohlmeister et al., 2010b; Lechleitner et al., 2016), and in-cave fractionation processes (e.g., Mattey et al., 2016; Spotl et al., 2005) may have an influence and little is known about the relative magnitude of these processes. Besides the stable C isotopes, radiocarbon (^{14}C), decaying with a half-life of ~5700 yrs (Kutschera, 2013), can be a valuable tool in speleothem research (e.g., Bajo et al., 2017; Lechleitner et al., 2016). So far, this isotope has not been fully exploited in speleothem science, mostly due to the time-consuming sampling and processing as well as the

comparably high costs associated with these analyses. However, recently both issues have been considerably improved by invention (Welte et al., 2016a; Welte et al., 2016b) and advances in laser ablation coupled to accelerator mass spectrometry (LA-AMS; Welte et al., 2017; Yeman et al., 2019), which can be well applied to carbonate material.

We investigated a stalagmite that grew in the Spannagel cave system (Tyrol, Austria; Spötl et al., 2004) by means of C isotope systematics. This high-alpine cave system was investigated in many studies in the context of palaeoclimate and palaeoenvironmental research mostly using O isotopes and growth phases as proxies (e.g., Fohlmeister et al., 2013; Spötl and Mangini, 2010). The gneiss covering the cave-bearing marble contains interspersed fine-crystalline pyrite (Spötl et al., 2004) and is topped by a thin soil layer with sparse vegetation. It was hypothesized that the oxidation of pyrite contributes considerably to the dissolution of the host-rock marble and, hence, to the growth of stalagmites and flowstones, in particular during cold climate periods when there is no soil present at this high altitude (Spotl and Mangini, 2007). During some interglacials including the Holocene, when Alpine soils are present in the catchment of the cave´s drip water, sulfide oxidation and soil-derived CO_2 may operate in tandem. Consequently, the stable C isotope signal of stalagmites from this cave is expected to be complexvary significantly.

The aim of this study is to gain deeper insights into the climatically driven C dynamics in this cave by high spatially resolved ^{14}C analyses of a Holocene stalagmite. This study takes advantage of the recently introduced method of LA-AMS (Welte et al., 2016a; Welte et al., 2016b), which reaches a similar spatial resolution as micro-milling for stable isotope analysis (e.g., Spötl and Mattey, 2006). Using the combined ^{14}C and $\delta^{13}C$ records measured in this study as well as the previously published $\delta^{18}O$ signal (Fohlmeister et al., 2013), we explore the key processes influencing the carbon isotope composition of speleothems in this cave and gain a better understanding of the potential and limits of ^{14}C analysis of carbonates using LA-AMS.

2 Radiocarbon and dead carbon fraction

In most karst systems, dissolution of the carbonate host rock is driven by soil-derived carbonic acid forming in meteoric precipitation seeping through the soil. In this case, the two major soil-derived C sources contributing to the $\delta^{13}C$ values of the speleothem are pedogenic CO_2 from the degradation of soil organic matter (SOM, Trumbore, 2000) and root respiration (Cerling, 1984) that acidifies the meteoric water as it percolates through the soil. Recently, evidence was found for a potential additional C source stemming from CO_2 derived from the oxidation of "old" organic matter (OM) in the deep vadose zone (Bergel et al., 2017; Noronha et al., 2015). The water charged with carbonic acid then dissolves the host rock $CaCO_3$. In some karst systems, the oxidation of pyrite has shown to contribute to the acidification of the seepage water and hence to speleothem formation (e.g., Spötl et al., 2016). All of those C-pools have different characteristics with respect to their stable and radiocarbon radioactive isotope signatures (Figure 1Fig. 1).

91
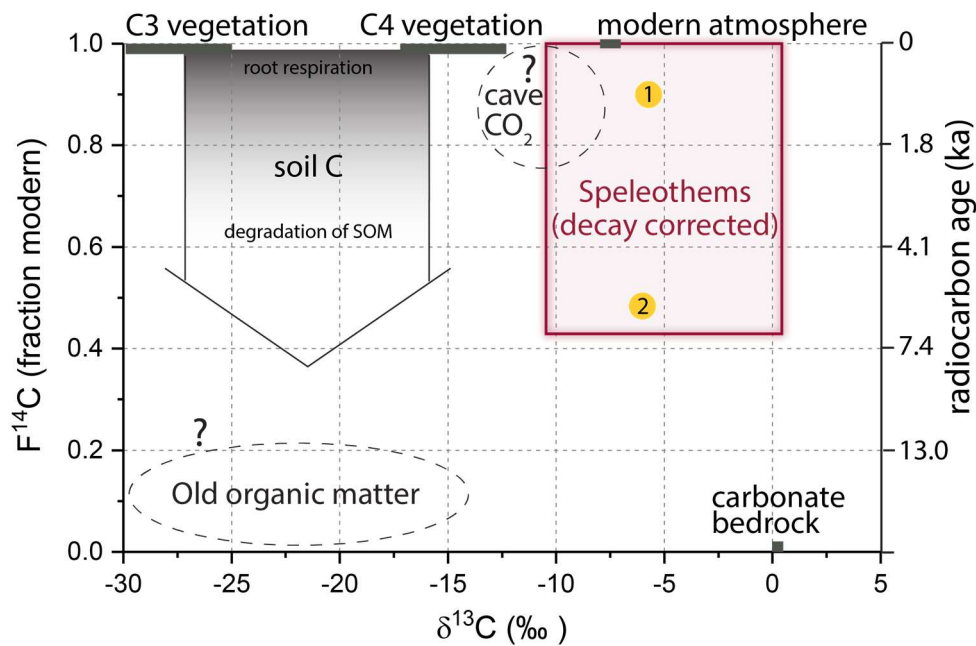
Figure 1: Carbon isotopic signatures of carbon-bearing reservoirs in karst systems. Yellow circles mark speleothem-C resulting from different processes: 1. $CaCO_3$ dissolution via soil CO_2-derived carbonic acid. 2. Deep organic carbon contribution to seepage water feeding speleothems (adapted from Fairchild and Baker (2012)).

When working with radiocarbon in speleothems it is important to determine the reservoir effect (Genty and Massault, 1997). If a radiocarbon-independent chronology for the stalagmite exists, the reservoir effect, which is often termed dead carbon fraction (dcf), can be derived through comparison of the measured ^{14}C profile in the stalagmite ($F^{14}C_{stal}$) with the ^{14}C atmosphere's signature ($F^{14}C_{atm}$) of the same time (Genty and Massault (1997)):

$$dcf = \left(1 - \frac{F^{14}C_{stal}}{F^{14}C_{atm}}\right) \cdot 100\% \qquad (1)$$

Values for dcf range from a few % up to 70% (Bajo et al., 2017; Southon et al., 2012) and commonly vary within a single speleothem with time (Bajo et al., 2017; Noronha et al., 2014; Therre et al., 2020). The magnitude of the dcf is influenced by multiple factors, such as the age of soil OM, contributing to soil gas CO_2 production (Fohlmeister et al., 2011b) and consequently altering the ^{14}C concentration in the stalagmite. Also the CO_2 partial pressure (pCO_2) in the soil plays an important role, with a complex relationship between the amount of soil gas pCO_2 and the dcf (Fohlmeister et al., 2011b). Additionally, the conditions of karst dissolution, i.e. open vs. closed system (Fohlmeister et al., 2011a; Hendy, 1971), affect the dcf. In a more open system, the dcf is low because the percolating water can continuously exchange C isotopes with the soil gas CO_2 leading to a ^{14}C concentration in the stalagmite that is dominated by the near-atmospheric soil ^{14}C signature (Southon et al., 2012). In a more closed system, this exchange is inhibited with the extreme case being a completely closed system, where for each mole of carbonic acid one mole of $CaCO_3$ is dissolved resulting in a dcf of up to 50% (Hendy, 1971). Fractionation and C exchange between cave air CO_2 and dissolved inorganic carbon (DIC) in drip water~~gas exchange processes in the cave~~ are also potential candidates for modulation of the dcf. These main factors driving the dcf in turn are influenced by numerous parameters such as hydrological and environmental conditions above the cave. Several studies (e.g., Bajo et al., 2017; Fohlmeister et al., 2010a; Griffiths et al., 2012; Lechleitner et al., 2016; Noronha et al., 2014) showed that during periods of increased rainfall the dcf in the stalagmite is enhanced. A likely explanation is a shift towards more closed-system conditions (**Error! Reference source not found.**~~Table 1~~) under

higher meteoric precipitation regimes. It was argued, that under more humid (arid) conditions the pore spaces in soils are clogged with (devoid of) water, leaving less (more) opportunity for C-exchange processes between dissolved inorganic C species and soil gas CO_2 (Fohlmeister et al., 2010).

An increasing number of cave systems have been reported where carbonate dissolution occurs even if no significant soil exists above the cave, indicating climatic conditions less suited for the existence of vegetation cover. Acidic conditions in the seepage water are achieved via oxidation of pyrite or other sulfide minerals disseminated in the bedrock (Bajo et al., 2017; Lauritzen, 2001; Spötl et al., 2016). In this case the C isotope composition in the drip water is dominated by the bedrock, and the dcf is therefore expected to be relatively high (>50%). Under those conditions the $\delta^{13}C$ values of the speleothems reflect those of the (marine-derived) bedrock, i.e. are shifted closer to 0‰ compared to lower $\delta^{13}C$ values of speleothem $CaCO_3$ of around -12 to -10‰ for cave systems with a soil and vegetation cover. An overview of relevant processes as well as the resulting dcf and $\delta^{13}C$ are summarized in **Error! Reference source not found.**~~Table 1~~.

Table 1 Simplified summary of expected $\delta^{13}C$ (assuming C3 vegetation cover) and dcf values in stalagmite $CaCO_3$ for different dominant processes. In many karst systems various combinations of these processes complicate the interpretation. This table is a compilation of data from Fohlmeister et al. (2011b); Spötl et al. (2016); Therre et al. (2020)

Process		Expected $\delta^{13}C$ (‰)	Expected dcf (%)
Carbonate dissolution via carbonic acid	open-system	< -10‰	Comparably low, i.e. around 10%
	closed-system	> -10‰	Comparably high, i.e. close to 50%
Carbonate dissolution via oxidation of pyrite		Close to 0‰	Very high, i.e. > 50%
"Old" OM contribution to seepage water acidification		< -10‰	Shift towards higher values (> 50% possible)

3 Materials & Methods

3.1 Sample

Spannagel cave is located in the Tux Valley (47.08028°N, 11.67167°E; Zillertal Alps, western Austria) and opens at 2531 m above sea level. It forms a more than 12 km-long system of galleries and short shafts, which developed in a Jurassic marble tectonically overlain by gneiss. This superposition does not only allow for high-precision U-series dating of stalagmites due to their relatively high U contents, but also gives rise to carbonate dissolution via sulfuric acid stemming from pyrite oxidation. The thin alpine soil provides an additional pedogenic source of acidity and the interplay between the two processes is reflected by highly variable stable C isotope values as well as dcf in Spannagel speleothems. Stalagmite SPA 127 was found in the eastern part of the cave system, which was never ice-covered during the Holocene (Fohlmeister et al., 2013). The stalagmite grew from 8.45 to 2.24 ka BP with an average growth rate of ~~approximately~~ 25 μm/a based on~~as confirmed by~~ nine U/Th-ages (Fohlmeister et al., 2013). There is no macro- and microscopic evidence for the existence of hiatuses in this specimen. Further evidence for the absence of hiatuses is provided by two additional speleothems, SPA 12 and SPA 128, from the same cave are partly coeval with SPA 127. These additional speleothems have a higher dating density in parts, where SPA 127 has only a few radiometric U-Th dating points and also do not show evidence of hiatuses

148   (Fohlmeister et al., 2013). In combination with the well replicated stable O isotope signals we are confident that

149   the growth of SPA 127 was not ~~affected~~ interrupted by hiatuses.

150   The 15 cm-long polished slab of the stalagmite analyzed in this study was first used for stable oxygen and carbon

151   isotope analysis where sampling was performed along the extension axis. For LA-AMS analysis, the same section

152   was used but broken in two pieces at a distance from top (dft) of approximately 10 cm, which will be referred to

153   as "top piece" and "bottom piece".

154   1.   Stable isotope analysis

155   Subsamples for stable carbon isotope analysis were micromilled at 100 μm increments and measured using an

156   automated online carbonate preparation system linked to a triple collector gas source mass spectrometer

157   (Delta^{plus}XL, ThermoFisher, Bremen, Germany) at the University of Innsbruck. Values are reported relative to the

158   Vienna Pee Dee Belemnite standard. The long-term precision of the δ^{13}C values (1 standard deviation of replicate

159   analyses) is 0.06% (Spötl, 2011). The respective δ^{18}O values have been published earlier (Fohlmeister et al., 2013).

160

3.2 Radiocarbon analysis using LA-AMS

161

162   By focusing a laser on the surface of a solid sample at sufficiently high energy densities, a small portion of material

163   is ablated and can be used for trace element or isotopic analysis allowing for fast and spatially resolved analysis

164   (Gray, 1985; Koch and Gunther, 2011). ^{14}C analysis of SPA 127 was performed at the Laboratory of Ion Beam

165   Physics, ETH Zurich, Switzerland, by LA coupled with AMS (Welte et al., 2016a; Welte et al., 2017). For this

166   study, a slightly modified LA-AMS setup was used reaching a smaller spot size (75x140 μm^2) and higher energy

167   densities of up to 8 J/cm^2 allowing for increased signal intensities, i.e. ^{12}C-currents. With LA-AMS a quasi-

168   continuous data stream is produced at 10 sec intervals in the AMS. This is the minimal integration time of the

169   AMS and together with the laser spot width d and the scanning velocity v defines the spatial resolution R according

170   to R = d + v · 10 sec.

171   LA-scans were placed as close as possible to the stable isotope tracks in order to facilitate matching between the

172   two data sets (Fig. 2). However, the LA-AMS setup does not permit to place laser tracks close to the rim of samples

173   causing an offset between the two sampling lanes of approximately 5 mm. Speleothem growth layers are often

174   curved, resulting in a potential offset between stable isotope and radiocarbon data of up to several hundred

175   micrometers, with the outer LA-scan appearing somewhat older than the stable isotope record. Since the curvature

176   of the growth layers is most likely variable, a constant correction factor has not been applied.

177   On the "top piece" of SPA 127 two subsequent scans in opposite direction were performed, first from young to

178   old (T1) and then vice versa (T2) on the same track with a scanning velocity of 20 μm/s and a laser energy density

179   of approximately 5 J/cm^2. On the "bottom piece" a total of three analyses were performed: the initial scan from

180   old to young (B1: 10 μm/s, 1-2 J/cm^2) was followed by a second repeated scan from bottom to top (B2: old to

181   young, 25 μm/s, 8 J/cm^2) after removing the top ~0.5 mm of the sample surface by mechanical polishing. The

182   second scan was necessary to ensure that the unusual ^{14}C signature observed in the oldest part of the stalagmite

183   during the first scan (see section ~~"Results"~~4) was not the result of a potentially contaminated surface. A final third

184   analysis (B3) consisting of two scans performed in opposite directions was performed at 20 μm/s and 5 J/cm^2.

185   Processing of the raw ^{14}C data was performed using in-house standards also analyzed by LA-AMS for blank

186   subtraction and standard normalization (marble, F^{14}C = 0 and coral standard, F^{14}C = 0.9445 ± 0.0018)~~.~~ and a

187   conventional fractionation correction to a δ^{13}C of -25‰ was applied (Stuiver and Polach, 1977). A Savitzky-Golay

188   (SG) filter is applied to the recorded ^{14}C signal of B3, which is a smoothing method that reduces noise while

189 maintaining the shape and height of peaks (Savitzky and Golay, 1964). In brief, a polynomial is fitted to a sub-set
190 of the data points and evaluated at the center of the approximation interval. Two parameters, namely the number
191 of points defining the approximation interval and the maximum polynomial order, can be defined. The smoothing
192 has been applied to the two sub-scans of B3 (from "old to young" and vice versa) as well as to the combined data
193 to ensure robustness of the filter. Corresponding uncertainties are estimated from the square root of the sum of the
194 squared difference between the measured F^{14}C value and the SG fit at each point within the interval. This value is
195 then divided by the square root of the difference between the interval length (number of data points) and the
196 maximum order allowed for the polynomial, which is equivalent to the degree of freedom.
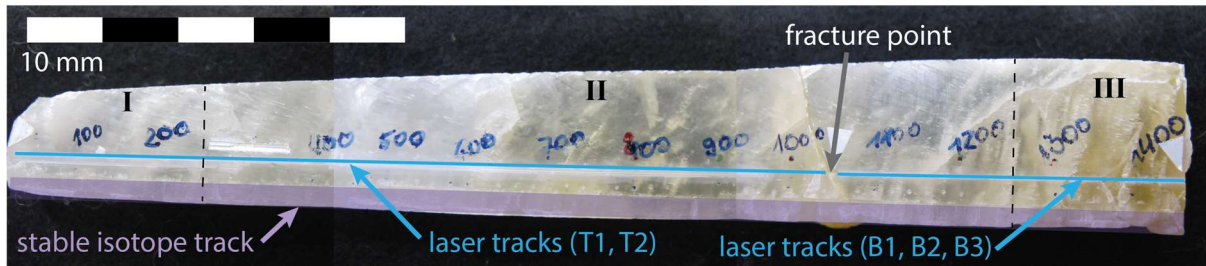
197

198 *Figure 2: Polished slab of SPA 127 (top is left).* ~~*Top and bottom piece with I*~~*LThe location~~s~~ of the stable isotope track ~~are~~*
199 ~~*marked in purple*~~ *and of the LA-AMS ~~test~~ tracks are marked in purple ~~in~~ and blue, respectively ~~(the tracks corresponding to~~*
200 ~~*the data presented in this work were placed next to the test tracks)*~~. *The total length of the slab is 14.6 cm. Roman numbers and*
201 *dashed black lines mark the three sections discussed separately.*

4 Results

4.1 Dead carbon fraction

204 ^{14}C results for both pieces of SPA 127 (T1, T2 and B3) are reported as dcf (blue line in Fig. 3 a and Fig. S8 a).
205 ~~From the~~Using the ^{14}C profile of the speleothem, the StalAge (Scholz and Hoffmann, 2011) age-depth model ~~was~~
206 applied to previously published U-Th data (Fohlmeister et al., 2013) and the known ^{14}C content of the atmosphere
207 during the Holocene (Reimer et al., 2016), ~~and~~ the dcf was calculated according to equation (1) for the 1402
208 radiocarbon data points (Figure 3~~Fig. 3~~ a~~A~~). A Savitzky-Golay (SG) filter was applied (interval: 21, maximum
209 polynomial order: 2) and for comparison the δ^{18}O and δ^{13}C data are shown in the same graph (Figure 3~~Fig. 3~~ a and
210 b). The U-Th-dates and the corresponding average growth rate calculated using StalAge are displayed in Figure
211 3~~Fig. 4~~ c.

4.2 Stable C isotopes

213 The previously published δ^{18}O values (Fohlmeister et al., 2013) and unpublished δ^{13}C data (this study) are shown
214 in Figure 3~~Fig. 3~~ a and b, respectively. A large amplitude and fast changes ranging from -8‰ to +1‰ characterize
215 δ^{13}C throughout the entire length of the speleothem but are especially pronounced between 30 and 130 mm (ca.
216 4.0 - 8.1 ka BP). Layers exhibiting a comparably stable δ^{13}C occur at the top and bottom of SPA 127, specifically
217 ranging from 4~~0~~ to 25 mm (ca. 2.6 and 3.7 ka BP) and from 13~~0~~25 to 14~~0~~50 mm (ca. 8.1 - 8.4 ka BP).

5 Discussion

219 The interpretation of the results on C isotopes in SPA 127 will be divided in three ~~main parts~~sections that
220 correspond to three sections identified on the speleothem based on their δ^{13}C characteristics, i.e., two periods of
221 comparably stable - δ^{13}C before 8 ka BP and after 3.5 ka BP and the interval in between with large and rapid
222 fluctuations.

5.1 Old section of SPA 127 (8.5-8.0 ka BP)

In the oldest part of SPA 127, the dcf is comparably high (~60%), while $\delta^{13}C$ is relatively depleted with values lower than -5‰ on average. Although the reservoir effect is extremely high, in principle the obtained C-isotope composition can be explained without a major contribution of pyrite oxidation. The relatively low $\delta^{13}C$ value of -5‰ actually contradicts this mode of host rock dissolution but is in line with a sparse C3 vegetation ($\delta^{13}C \approx$ -25‰) above the cave and host rock dissolution under nearly closed conditions (compare Fig. 4Fig. 4 cC and dD). The stoichiometry of $CaCO_3$ dissolution by carbonic acid predicts that only about half of the C in the solution is derived from the host rock under nearly completely closed conditions. Given that the Jurassic host rock is devoid of ^{14}C, the biogenic component must be older than the contemporaneous atmosphere to allow dcf values larger greater than 50%. Thus, in addition to the atmospheric radiocarbon contribution from living vegetation, which contributes atmospheric radiocarbon, an "old" OM source, which respires radiocarbon-depleted CO_2, is required to explain the depleted $\delta^{13}C$ values and elevated dcf. Such "old" OM is also argued to have contributed to the radiocarbon reservoir effect of Moomi Cave (Socotra Island) during the last glacial period (Therre et al., 2020). Observations from other cave and karst systems also point to important C pools deep in the vadose karst, e.g., (Benavente et al., 2010; Bergel et al., 2017; Breecker et al., 2012). Nevertheless, in a sparsely vegetated high elevation region this is the first finding of this kind.

The speleothem growth phase prior to 8.0 ka falls coincides with the early Holocene thermal maximum, which is also reflected by the depleted $\delta^{18}O$ values hinting towards higher temperatures (Fohlmeister et al., 2013; Mangini et al., 2005). Warmer periods likely favor microbial decomposition of, e.g., OM present in the epikarst below the soil zone, which leads to an increase in pCO_2 and, hence, more acidic water. In turn, more $CaCO_3$ can be dissolved giving rise to higher speleothem growth rates, which is indeed observed in this period (Figure 3Fig. 3, orange shaded area). Thus, growth rate and the C-isotope composition of stalagmite SPA 127 are in agreement with the presence of a deep OM reservoir in the karst system above the cave.
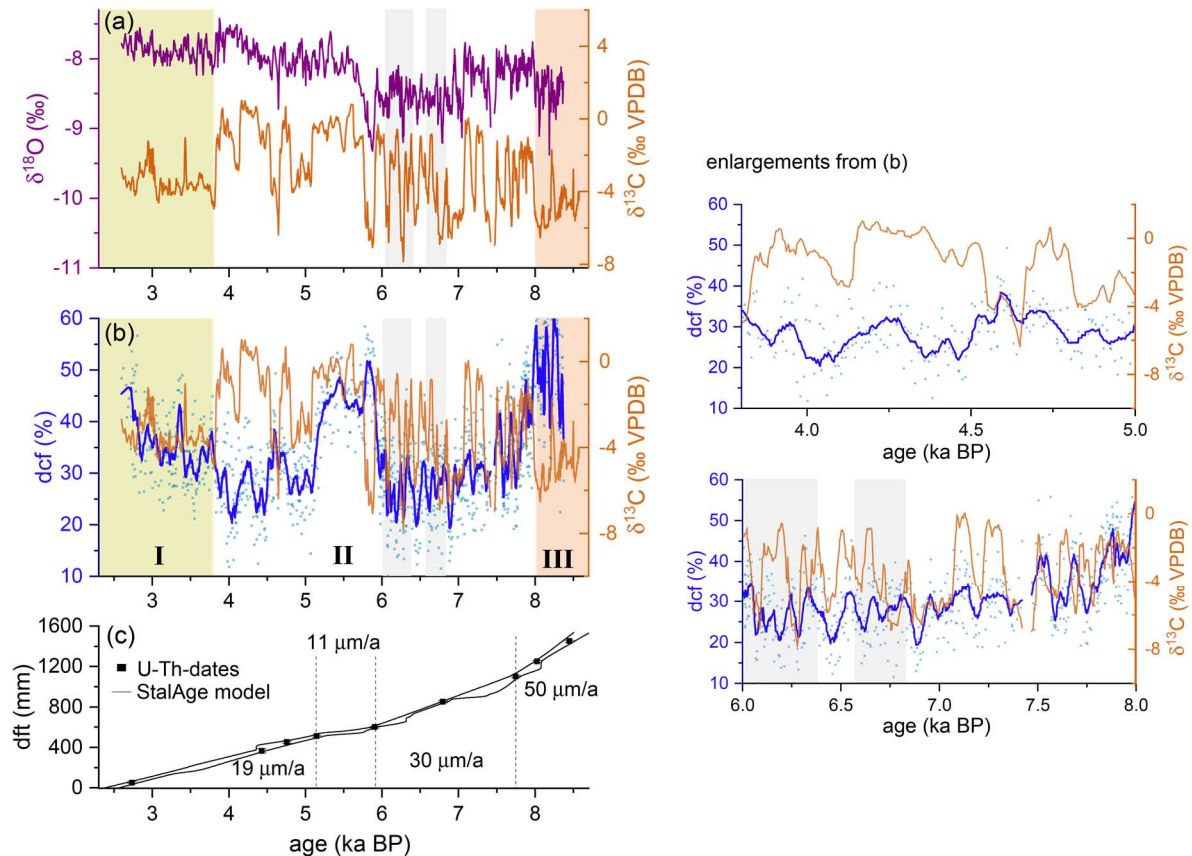
246

247 *Figure 3: ~~Dcf (light blue dots) with a 21 point SG filter (dark blue line) plotted against age and compared to (A)~~ δ¹⁸O*

248 ~~*(represented by the purple*~~*green line)* *(Fohlmeister et al., 2013) compared to δ13C (orange line) and (~~B~~b) dcf (light blue dots)*

249 *with a 21 point SG filter (dark blue line) plotted against age and compared to δ13C ~~(orange line)~~. The yellow, white and orange*

250 *shaded areas represent phases with distinct stable isotope characteristics. Roman numbers indicate the three subsections*

251 *discussed in the text.~~Details can be found in the text.~~ Light grey shaded areas mark regions where the SG filter was determined*

252 *with lower confidence. Enlargements of this graph are shown in the right panel. (~~C~~c) Growth history of SPA 127 obtained by*

253 *StalAge applied to dated depths (black squares, errors are smaller than the symbol size). Numbers represent average growth*

254 *rates of~~s~~ the individual sections.*

5.2 Rapid changes in dcf and stable C isotopes (8.0 to 3.8 ka BP)

256 The growth rate was reduced in this period compared to the previous one (Fig. 3 c). This either suggests that

257 meteoric precipitation or the amount of soil-derived C were reduced, both resulting in a smaller amount of

258 dissolved carbonate transported to the cave. The low δ¹³C values of the first growth period were superseded by

259 rapid and very large variations of δ¹³C. This pattern is complex and its interpretation is difficult, as this behavior

260 has not been observed elsewhere. Processes in the soil and karst as well as in-cave processes ~~have to be taken into~~

261 ~~consideratio~~must be considered~~n~~. High-resolution LA-AMS ¹⁴C measurements in conjunction with O isotope data

262 and growth rate changes, however, greatly assist in disentangling the driving mechanism(s) for these δ¹³C

263 variations. The dcf between 8.0- ~~a~~and 3.8 ka BP is generally lower than in the older section. This means that either

264 the aged OM in the karst was depleted or its degradation was reduced, possibly due to a reduction in meteoric

265 precipitation (as deduced from growth rate reduction). Both reasons, less meteoric precipitation and a depleted

266 deep OM pool, would well explain the observed reduction in growth rate. The only speleothem C sources available

267 in this period were consequently the close-to-modern SOM and the radiocarbon-free host rock.

The dcf record shows a strong and rapid increase around 6 ka and a rapid decrease back to pre-6 ka levels at around 5 ka (Fig. 3 b). The increase in dcf occurs at the same time as a significant decrease in $\delta^{18}O$, but dcf remains elevated when $\delta^{18}O$ jumps back again shortly after. Instead, the decrease in dcf at 5 ka occurs contemporaneously with a $\delta^{13}C$ decrease after $\delta^{13}C$ values remained at elevated values for nearly a millennium. The reason for such a behavior of the dcf remains elusive. In this section, we focus on the cause of the large and rapid jumps in $\delta^{13}C$ by ~~testing~~ proposing two hypotheses.

Hypothesis 1: Processes above the cave, i.e. different carbonate dissolution processes, cause the rapid switching

Two different processes may have caused carbonate dissolution at Spannagel cave in this period. The first involves soil CO_2-derived carbonic acid (from root respiration and microbial decomposition of SOM) while the second process operates via sulfuric acid formed by pyrite oxidation (compare ~~Fig. 4~~Fig. 4 ~~a~~A and ~~b~~B). During times when the first process dominates, the stable carbon isotopic composition of stalagmites is strongly influenced by C from the soil shifting $\delta^{13}C$ towards more negative values. At the same time, the dcf is expected to be relatively low (at least <50%) as the comparably ^{14}C-rich soil C contributes significantly to the signal. In contrast, pyrite oxidation leads to more positive $\delta^{13}C$ values in the stalagmite corresponding to the $\delta^{13}C$ composition of the host rock, as the $\delta^{13}C$-depleted biogenic source contributes little or even no C (Bajo et al., 2017; Spötl et al., 2016). Under these conditions, the dcf should increase to values close to 100% if the comparably modern soil contribution is absent. If the observed $\delta^{13}C$ variations are caused by rapid alternation between both processes, a positive correlation between $\delta^{13}C$ and the dcf has to be expected, with extreme values in the dcf as outlined above. However, no significant long-term positive correlation for the two data series, i.e. $\delta^{13}C$ and dcf, is observed (Fig. S10) and extreme ~~dcf~~DCF values are not observed. A robust comparison of both data sets is impeded because of the different spatial offset of the two measurement tracks from the growth axis. The radiocarbon track is located ca. 5 mm further from the central growth axis than the stable isotope track (~~Figure 2~~Fig. 2). Growth layers cannot be identified, but the small stalagmite diameter suggests steeply dipping layers resulting in an apparent shift of the dcf towards older ages relative to $\delta^{13}C$. Indeed, such a delay is observable when comparing details in the two data series (~~Figure 3~~Fig. 3 b). ~~Taking a~~Considering the potential offset between the two records ~~into account~~ (see ~~Materials & Methods~~section 3), a ~~positive correlation~~high degree of similarity between main features in $\delta^{13}C$ and dcf are observable for the middle period, especially between 8 and 6 ka and also partly between 5 and 3.8 ka BP. Those phases are interrupted by the interval of the previously described strong increase in dcf.

The large swings in $\delta^{13}C$ suggest frequent switches between the carbonate dissolution mechanism from carbonic acid dissolution to pyrite oxidation. However, this is expected to be accompanied by an increase of the dcf to 100% because of the diminishing ^{14}C-rich soil signature, which, however, is not observed. Generally, the dcf is even smaller than in the youngest and oldest sections of the stalagmite, i.e. after 3.8 ka and before 8 ka BP. ~~The correlation between dcf and $\delta^{13}C$ suggests that there might have been a C~~changes between open and closed carbonate dissolution regimes are expected to result in a positive relationship between the dcf and $\delta^{13}C$, which is observed in SPA 127. However,~~, but~~ the magnitude of $\delta^{13}C$ variations ~~found in SPA 127~~ is too large to be explained by a change of the dissolution regimes~~larger than if triggered by this process~~ even when considering the extreme switch~~changing~~ from ~~a~~ completely open to ~~a~~ completely closed ~~system~~ (Hendy, 1971; Fohlmeister et al., 2011). Thus, additional processes in the cave most likely caused this unusual behavior and the high-magnitude and high-frequency $\delta^{13}C$ variations.

CARBONATE DISSOLUTION MECHANISM ALTERNATING BETWEEN SOIL CO₂ AND SULFIDE OXIDATION
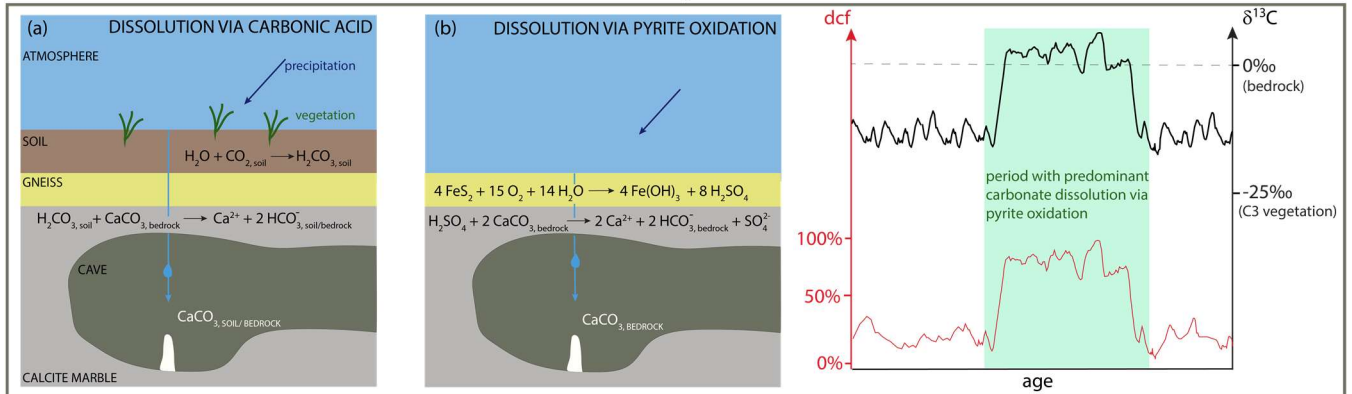
CARBONATE DISSOLUTION MECHANISM: OPEN vs. CLOSED
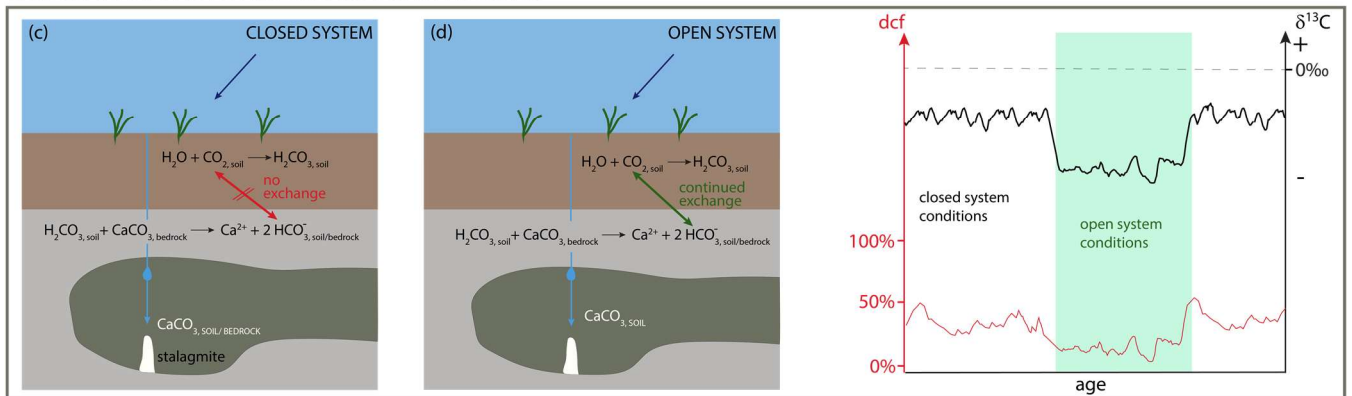
PROCESSES IN CAVE: FRACTIONATION
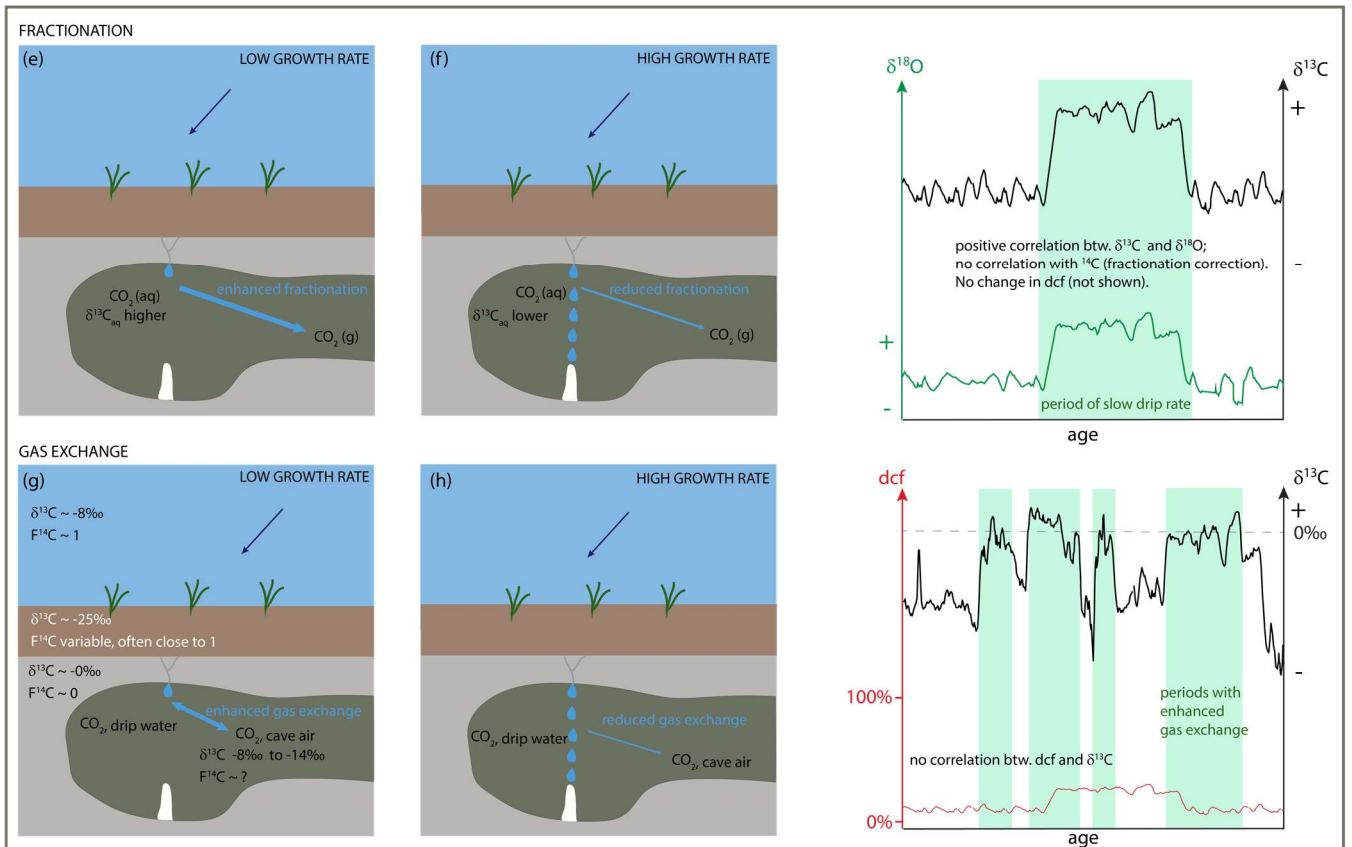
309   *Fig. 4 Overview of different processes that can influence F¹⁴C and δ¹³C in speleothems. For details see text.*

310   • **Hypothesis 2:** Processes in the cave cause the rapid switching

311 A major factor influencing the carbon isotope composition of stalagmites are fractionation processes (compare
312 Fig. 4Fig. 4 eE and fF), which occur during degassing of CO_2 and precipitation of $CaCO_3$ from the solution. Fast
313 dripping results in fast growth and leaves less time for fractionation or C isotope exchange (compare Fig. 4Fig.
314 4 gG and hH) and vice versa (e.g., Fohlmeister et al., 2018; Scholz et al., 2009). In addition, the difference in pCO_2
315 between water and cave-air CO_2 can also influence isotope fractionation and C exchange processes. In the middle
316 part of SPA 127, the average growth rate decreased to ≤ 30 µm/a, which is significantly lower than in the oldest
317 section (50 µm/a). As discussed earlier, the reduction in growth rate might have been partly induced by reduced
318 meteoric precipitation resulting in slower drip rates or by reduced soil or karst CO_2 concentrations leading to less
319 dissolved host rock $CaCO_3$. In addition, a lower or absent contribution of an "old" OM reservoir in the karst would
320 have led to a lower pCO_2 difference between the CO_2 concentration in the drip water and cave air, which favors
321 an increase in $\delta^{13}C$ through fractionation and C isotope exchange processes in the cave. We hypothesize that the
322 rapid changes in $\delta^{13}C$ might correlate with short-term changes in growth rate, which cannot be resolved by the
323 available U-Th chronology, enabling or disabling isotope fractionation and C exchange between cave air CO_2 and
324 DIC in drip watergas exchange in the cave that are described in the following two paragraphs.

325 (i)   Changes in isotope fractionation effects

326 During periods of slow growth, fractionation processes can significantly alter the isotopic composition of the
327 stalagmite. During CO_2 degassing from the drip water, the lighter molecules are preferentially transferred
328 into the gas phase resulting in a solution enriched in heavy isotopes. Indeed, recent experiments (Fahrni et
329 al., 2017) support earlier findings that fractionation of radiocarbon relative to ^{12}C is about twice as large as
330 for ^{13}C relative to ^{12}C (Stuiver and Robinson, 1974). However, as radiocarbon measurements are corrected
331 for fractionation effects via $\delta^{13}C$ values, it is impossible to detect a potential correlation between the two
332 isotopes due to fractionation effects. However, potential fractionation affecting $\delta^{13}C$ also influences $\delta^{18}O$ and
333 can be confirmed by a positive correlation between stable C isotopes and O isotopes, e.g. (Dreybrodt, 2008;
334 Polag et al., 2010). Applying a running correlation coefficient between $\delta^{13}C$ and $\delta^{18}O$ is a powerful tool to
335 detect fractionation changes through time (Fohlmeister et al., 2017). 11-point running correlation coefficients
336 calculated for the two time series of SPA 127 show no stalagmite sections with a high correlation coefficient,
337 but vary without any obvious pattern between -1 and +1 (compare Fig. S10, bottom panel). Thus,
338 fractionation was most likely not the main process causing the large variations in $\delta^{13}C$, but may have played
339 a minor role during some periods.

340 (ii)   Prior calcite precipitation (PCP)

341 PCP can have an effect on $\delta^{13}C$, even a large ones as observed for our stalagmite. While this would not have
342 an effect on ^{14}C, we would expect that $\delta^{18}O$ should show a similar behavior, which is not the case (Fig. 3 a).
343 Thus, we can safely assume, that PCP is not responsible for the rapid changes observed in SPA 127.

344 (iii)   C exchange between cave air CO_2 and DIC in drip water. Gas exchange processes

345 Another process that is a potential candidate for causing the behavior observed in SPA 127 in this interval is
346 the C isotope exchange between CO_2 of the cave air and C dissolved in the drip water. The g C exchange
347 between cave air CO_2 and DIC in drip wateras exchange process may be the dominant process if the
348 stalagmite growth rate is sufficiently low and when drip interval is long, meaning that 95% of the $CaCO_3$

precipitated either via PCP or on the stalagmite (Guo, 2020), and/or the differences between the pCO_2 of the water and cave air is small (Hendy, 1971; Scholz et al., 2009). In this case, the C isotopic composition of the drip water when reaching the top of the stalagmite depends mainly on the initial $\delta^{13}C$ of drip water and on the degree of C isotope exchange with the cave atmosphere. Spannagel Cave is well ventilated throughout the year with cave air $\delta^{13}C$ values of -10 to -11‰ (Tochterle et al., 2017), which is significantly lower than that of the atmosphere, i.e. approximately -8‰ (Keeling et al., 2010). These more negative values are a hint towards a contribution from soil air. The following assumptions were made: the $\delta^{13}C$ of drip water is composed of two biogenic C sources ($\delta^{13}C \sim$ -25‰) and host rock ($\delta^{13}C \sim$ +2.80‰) and about 20 - 30% are derived from the host rock (based on the dcf in this interval). Accounting for about 10‰ to 11‰ fractionation between soil gas CO_2 and HCO_3^- during the transition of soil gas CO_2 to dissolved inorganic carbon (DIC), the initial drip water, which was feeding the stalagmite, had a $\delta^{13}C$ value between -11.5 and -9‰ (Mook et al., 1974). Considering Rayleigh fractionation effects in the cave, carbonate $\delta^{13}C$ values of -8‰ appear feasible (Scholz et al., 2009, Deininger et al., 2012) without any exchange of C isotopes. C isotope exchange processes lead to water significantly enriched in ^{13}C. When cave air with $\delta^{13}C$ values around -11‰ exchanges with drip water, the C isotopic composition of the water will increase, as the transition of gaseous CO_2 to HCO_3^- involves a fractionation of about +10 to +11‰ at temperatures between 0 and 5°C (Mook et al., 1974). Thus, drip water in C isotopic equilibrium with cave air CO_2, which is the most extreme case, should have $\delta^{13}C$ values of -1 to 0‰. Precipitation of $CaCO_3$ from such water would result in $\delta^{13}C$ values of around 0 to +1‰ as observed for some short intervals.

Similar considerations can be applied to radiocarbon. If the cave ventilation is sluggish, $F^{14}C$ in the cave air will deviate from atmospheric values (i.e. $F^{14}C_{atm} \approx 1$) as it is influenced by other sources, such as soil air or CO_2 degassed from drip water, which both are depleted with respect to atmospheric values. In a recent study, cave air has been shown to be depleted in radiocarbon with values as low as $F^{14}C \approx 0.6$ (Minami et al., 2015). When the cave ventilation is not effectively changing the depleted radiocarbon towards more atmospheric values, C isotope exchange processes are not detectable using ^{14}C in speleothems. As isotopic fractionation is not important for radiocarbon (as explained above), C isotope exchange of DIC with cave air, which both have a similar radiocarbon content, would have no effect on the ^{14}C signal of the precipitated calcite.

~~In summary, combined high-resolution $\delta^{13}C$ and radiocarbon measurements are a valuable tool to shed new light on processes affecting C isotopes in the subsurface. Using well justified assumptions and first-order calculations of mixing and fractionation effects, in-cave C isotope exchange processes remain the only explanation for the rapid and high-magnitude $\delta^{13}C$ changes.~~

5.3 Interpretation of dcf and $\delta^{13}C$ in the youngest section of SPA 127 (3.8 to 2.5 ka BP)

In the youngest section of this stalagmite a behavior similar to the oldest section with respect to $\delta^{13}C$ and radiocarbon content is observed. From approximately 3.8 ka BP onward, the dcf increases slowly from about 20% to 50%. Correspondingly, $\delta^{13}C$ shows a lower variability than in the middle part with mean $\delta^{13}C$ values of -3‰ to -4‰, which is also comparable to the behavior observed for the interval > 8 ka BP. As $\delta^{13}C$ does not show any long-term trend as observed for the reservoir effect, we rule out a change to more closed carbonate dissolution conditions driving the increase in dcf. The only explanation that can lead to such an increase is an "old" C reservoir. We propose that climatic conditions changed such that this "old" OM pool in the karst, which was decoupled from the atmosphere, has become the main OM derived CO_2 source. This CO_2 resulted in acidification in a comparable

389 way as soil CO_2 enhancing carbonate dissolution and ultimately contributed to stalagmite $CaCO_3$. The isotopic [14]C
390 imprint, however, is significantly different to soil CO_2 causing the observed increase in dcf. Between
391 approximately 8 and 6 ka BP the Alps experienced a warmer climate than today (Ivy-Ochs et al., 2009; Nicolussi
392 et al., 2005). A study conducted by Nicolussi et al. (2005) in the Kauner valley, situated approximately 70 km west
393 of Spannagel Cave, showed that the timberline was significantly higher during that period (Figure 5Fig. 5**Error!**
394 **Reference source not found.**) supporting a warmer climate. Between 6 and 4 ka BP the timberline was comparable
395 to the present-day situation.
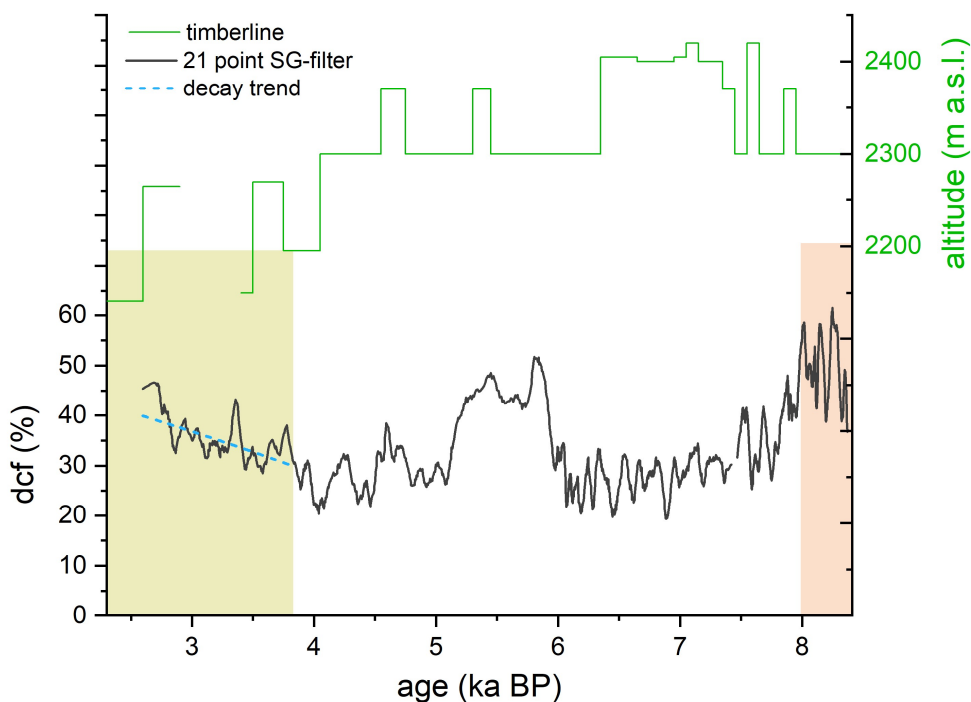
397 *Figure 5: Comparison of the dcf in stalagmite SPA 127 with the elevation of the timberline reconstructed for the Kauner*
398 *valley 70 km west of Spannagel Cave (green line, after Nicolussi et al. (2005)) with the dcf. Around 4 ka BP the timberline*
399 *started to decline which is concurrent with an increase in dcf, i.e., a decrease in initial [14]C. This decrease closely follows a*
400 *radiocarbon decay trend (dashed blue line). Green and red areas mark the three different time periods as indicated in Figure*
401 *3Fig. 4.*

402 It is expected that with the lowering of the timberline after ~4 ka the vegetation density decreased as well, which
403 should be reflected in the speleothem- $\delta^{13}C$ values. This, however, is not the case during this period pointing
404 towards a relatively stable contribution of soil-derived CO_2. Possibly, a certain proportion of plants that grew
405 during the early to mid-Holocene warm epoch died and the corresponding OM located in the deeper vadose zone
406 was initially stabilized due to reduced meteoric precipitation and later became mobilized due to enhanced microbial
407 activity. Considering the low mean annual temperatures at this high-alpine site, decomposition processes are most
408 likely slow, allowing OM to age during decomposition as indicated in a recent study by Shi et al. (2020). The
409 radiocarbon composition of the ageing SOM will closely follow a radiocarbon-specific exponential decay and is
410 responsible for the depleted radiocarbon concentration in soil gas CO_2. Depending on the contribution of root-
411 respired CO_2 of Alpine plants compared to the decomposed CO_2 from dead OM, the dcf will closely follow an
412 exponential decay, resembling that of the radiocarbon decay and thus would contribute to the observed increase of
413 the dcf. The closer the observed increase in the dcf follows that of a radiocarbon decay trajectory, the larger the
414 contribution of CO_2 from the aging SOM reservoir in relation to root-respired CO_2. Based on the observed rate of

415 increase in dcf, which compares well with the radiocarbon decay trend (blue dashed line in ~~Figure 5~~Fig. 5), we

416 suggest that the majority of DIC that contributed to the speleothem $CaCO_3$ had its origin in aged soil OM.

6 Conclusion

418 Combined stable carbon isotope and radiocarbon analyses of stalagmite SPA 127 provide a comprehensive picture

419 of the carbon dynamics at ~~the~~ Spannagel Cave. ~~With the~~Due to the novel LA-AMS technique, a highly spatially

420 resolved ^{14}C time series allows unprecedented insights into processes in this high-alpine karst system. Care has to

421 be taken when applying LA-AMS to stalagmites as epoxy resin used in sample preparation leads to distorted

422 results.

423 Results from this study allow to distinguish three intervals with different carbon dynamics:

424 (i) The interval before 8 ka BP is characterized by generally low and stable δ^{13}C values combined with a

425 comparably high dcf (>50%) pointing towards the existence of an "old" OM reservoir in the epikarst.

426 CO_2 emanating from this presaged C pool provides additional carbonic acid potentially enhancing

427 bedrock dissolution.

428 (ii) The interval between 8 and 3.8 ka BP is characterized by a strong variability in δ^{13}C with a generally

429 lower dcf suggesting that the "old" OM reservoir in the karst had either been exhausted or stabilized (less

430 production to aged respired soil/karst CO_2) possibly due to reduced meteoric precipitation. This is

431 supported by a lower stalagmite growth rate in this period. C exchange between cave air CO_2 and DIC in

432 drip water~~In-cave gas exchange processes~~ is~~are~~ the most likely explanation for the strong δ^{13}C variability,

433 as (i) bedrock dissolution mechanisms, i.e. pyrite oxidation vs. carbonic acid dissolution, are not

434 supported by the magnitude of changes in dcf and stable C, even though the temporal coherence indicates

435 that some of the δ^{13}C variations might be explained by the bedrock dissolution mode (open vs. closed

436 carbonate dissolution) and, (ii) fractionation processes in the cave cannot explain the large shifts as no

437 correlation between δ^{18}O and δ^{13}C is observed.

438 (iii) In the interval between 3.8 and 2.4 ka BP the comparably more stable δ^{13}C signature combined with an

439 increasing dcf hints towards a contribution from an ageing OM reservoir in the karst similar to the period

440 > 8 ka BP. This OM reservoir contributed to the stalagmite growth in this period due to warmer climatic

441 conditions. While the contribution of "old" OM in the oldest growth phase was stable, the youngest

442 section indicates an ageing of this reservoir.

Author contribution

444 CW, JF and CS conceptualized the content of this manuscript. CW, MW, BH carried LA-AMS measurements out,

445 CS conducted stable carbon isotope analyses. MW and LW developed the data reduction strategy. JF, CW and TE

446 interpreted the data and compared them to published records. CW prepared the manuscript with contributions from

447 all co-authors.

Competing interests

449 The authors declare that they have no conflict of interest.

Acknowledgements

JF acknowledge support from DFG grants FO 809/2-1 and FO 809/4-1. MW was supported by ETH Research Grant ETH-03 18-2. FTIR analyses were performed by Laura Hendriks. We also thank the two reviewers who helped ~~to improve~~improving this manuscript.

References

Bajo, P., Borsato, A., Drysdale, R., Hua, Q., Frisia, S., Zanchetta, G., Hellstrom, J., and Woodhead, J.: Stalagmite carbon isotopes and dead carbon proportion (DCP) in a near-closed-system situation: An interplay between sulphuric and carbonic acid dissolution, Geochimica Et Cosmochimica Acta, 210, 208-227, 2017.

Bar-Matthews, M., Ayalon, A., Kaufman, A., and Wasserburg, G. J.: The Eastern Mediterranean paleoclimate as a reflection of regional events: Soreq cave, Israel, Earth and Planetary Science Letters, 166, 85-95, 1999.

Benavente, J., Vadillo, I., Carrasco, F., Soler, A., Linan, C., and Moral, F.: Air Carbon Dioxide Contents in the Vadose Zone of a Mediterranean Karst, Vadose Zone Journal, 9, 126-136, 2010.

Bergel, S. J., Carlson, P. E., Larson, T. E., Wood, C. T., Johnson, K. R., Banner, J. L., and Breecker, D. O.: Constraining the subsoil carbon source to cave-air CO_2 and speleothem calcite in central Texas, Geochimica Et Cosmochimica Acta, 217, 112-127, 2017.

Breecker, D. O., Payne, A. E., Quade, J., Banner, J. L., Ball, C. E., Meyer, K. W., and Cowan, B. D.: The sources and sinks of CO_2 in caves under mixed woodland and grassland vegetation, Geochimica Et Cosmochimica Acta, 96, 230-246, 2012.

Cerling, T. E.: The Stable Isotopic Composition of Modern Soil Carbonate and Its Relationship to Climate, Earth and Planetary Science Letters, 71, 229-240, 1984.

Cheng, H., Edwards, R. L., Shen, C.-C., Polyak, V. J., Asmerom, Y., Woodhead, J., Hellstrom, J., Wang, Y., Kong, X., and Spötl, C.: Improvements in 230Th dating, 230Th and 234U half-life values, and U–Th isotopic measurements by multi-collector inductively coupled plasma mass spectrometry, Earth and Planetary Science Letters, 371, 82-91, 2013.

Cheng, H., Edwards, R. L., Sinha, A., Spotl, C., Yi, L., Chen, S., Kelly, M., Kathayat, G., Wang, X., Li, X., Kong, X., Wang, Y., Ning, Y., and Zhang, H.: The Asian monsoon over the past 640,000 years and ice age terminations, Nature, 534, 640-646, 2016.

Denniston, R. F., DuPree, M., Dorale, J. A., Asmerom, Y., Polyak, V. J., and Carpenter, S. J.: Episodes of late Holocene aridity recorded by stalagmites from Devil's Icebox Cave, central Missouri, USA, Quaternary Research, 68, 45-52, 2007.

Dreybrodt, W.: Evolution of the isotopic composition of carbon and oxygen in a calcite precipitating H_2O–CO_2–$CaCO_3$ solution and the related isotopic composition of calcite in stalagmites, Geochimica et Cosmochimica Acta, 72, 4712-4724, 2008.

Fahrni, S. M., Southon, J. R., Santos, G. M., Palstra, S. W., Meijer, H. A., and Xu, X.: Reassessment of the 13C/12C and 14C/12C isotopic fractionation ratio and its impact on high-precision radiocarbon dating, Geochimica et Cosmochimica Acta, 213, 330-345, 2017.

Fairchild, I. J. and Baker, A.: Speleothem science: from process to past environments, John Wiley & Sons, 2012.

Fairchild, I. J., Smith, C. L., Baker, A., Fuller, L., Spotl, C., Mattey, D., McDermott, F., and Eimp: Modification and preservation of environmental signals in speleothems, Earth-Science Reviews, 75, 105-153, 2006.

Fohlmeister, J., Arps, J., Spotl, C., Schroder-Ritzrau, A., Plessen, B., Gunter, C., Frank, N., and Trussel, M.: Carbon and oxygen isotope fractionation in the water-calcite-aragonite system, Geochimica Et Cosmochimica Acta, 235, 127-139, 2018.

Fohlmeister, J., Kromer, B., and Mangini, A.: The Influence of Soil Organic Matter Age Spectrum on the Reconstruction of Atmospheric C-14 Levels Via Stalagmites, Radiocarbon, 53, 99-115, 2011a.

Fohlmeister, J., Plessen, B., Dudashvili, A. S., Tjallingii, R., Wolff, C., Gafurov, A., and Cheng, H.: Winter precipitation changes during the Medieval Climate Anomaly and the Little Ice Age in arid Central Asia, Quaternary Science Reviews, 178, 24-36, 2017.

Fohlmeister, J., Scholz, D., Kromer, B., and Mangini, A.: Modelling carbon isotopes of carbonates in cave drip water, Geochimica Et Cosmochimica Acta, 75, 5219-5228, 2011b.

Fohlmeister, J., Schroder-Ritzrau, A., Spotl, C., Frisia, S., Miorandi, R., Kromer, B., and Mangini, A.: The Influences of Hydrology on the Radiogenic and Stable Carbon Isotope Composition of Cave Drip Water, Grotta Di Ernesto (Italy), Radiocarbon, 52, 1529-1544, 2010a.

Fohlmeister, J., Schroeder-Ritzrau, A., Spoetl, C., Frisia, S., Miorandi, R., Kromer, B., and Mangini, A.: The influences of hydrology on the radiovenic and stable carbon isotope composition of cave drip water, Grotta die Ernesto (Italy), Radiocarbon, 52, 1529-1544, 2010b.

Fohlmeister, J., Voarintsoa, N. R. G., Lechleitner, F. A., Boyd, M., Brandtstatter, S., Jacobson, M. J., and Oster, J. L.: Main controls on the stable carbon isotope composition of speleothems, Geochimica Et Cosmochimica Acta, 279, 67-87, 2020.

Fohlmeister, J., Vollweiler, N., Spotl, C., and Mangini, A.: COMNISPA II: Update of a mid-European isotope climate record, 11 ka to present, Holocene, 23, 749-754, 2013.

Genty, D. and Massault, M.: Bomb C-14 recorded in laminated speleothems: Calculation of dead carbon proportion, Radiocarbon, 39, 33-48, 1997.

Gray, A. L.: Solid Sample Introduction by Laser Ablation for Inductively Coupled Plasma Source-Mass Spectrometry, Analyst, 110, 551-556, 1985.

Griffiths, M. L., Fohlmeister, J., Drysdale, R. N., Hua, Q., Johnson, K. R., Hellstrom, J. C., Gagan, M. K., and Zhao, J. X.: Hydrological control of the dead carbon fraction in a Holocene tropical speleothem, Quat. Geochronol., 14, 81-93, 2012.

Guo, W.: Kinetic clumped isotope fractionation in the DIC-H2O-CO2 system: Patterns, controls, and implications, Geochimica et Cosmochimica Acta, 268, 230-257, 2020.

Hendy, C. H.: The isotopic geochemistry of speleothems—I. The calculation of the effects of different modes of formation on the isotopic composition of speleothems and their applicability as palaeoclimatic indicators, Geochimica et cosmochimica Acta, 35, 801-824, 1971.

Ivy-Ochs, S., Kerschner, H., Maisch, M., Christl, M., Kubik, P. W., and Schluchter, C.: Latest Pleistocene and Holocene glacier variations in the European Alps, Quaternary Science Reviews, 28, 2137-2149, 2009.

Keeling, R., Piper, S., Bollenbacher, A., and Walker, S.: Monthly atmospheric 13C/12C isotopic ratios for 11 SIO stations, Trends: a compendium of data on global change, 2010. 2010.

Koch, J. and Gunther, D.: Review of the state-of-the-art of laser ablation inductively coupled plasma mass spectrometry, Appl Spectrosc, 65, 155-162, 2011.

Kutschera, W.: Applications of accelerator mass spectrometry, International Journal of Mass Spectrometry, 349, 203-218, 2013.

Lachniet, M. S.: Climatic and environmental controls on speleothem oxygen-isotope values, Quaternary Science Reviews, 28, 412-432, 2009.

Lauritzen, S.-E.: Marble stripe karst of the Scandinavian Caledonides: an end-member in the contact karst spectrum, Slovenska akademija znanosti in umetnosti, 2001.

Lechleitner, F. A., Baldini, J. U. L., Breitenbach, S. F. M., Fohlmeister, J., McIntyre, C., Goswami, B., Jamieson, R. A., van der Voort, T. S., Prufer, K., Marwan, N., Culleton, B. J., Kennett, D. J., Asmerom, Y., Polyak, V., and Eglinton, T. I.: Hydrological and climatological controls on radiocarbon concentrations in a tropical stalagmite, Geochimica Et Cosmochimica Acta, 194, 233-252, 2016.

Mangini, A., Spötl, C., and Verdes, P.: Reconstruction of temperature in the Central Alps during the past 2000 yr from a δ18O stalagmite record, Earth and Planetary Science Letters, 235, 741-751, 2005.

Mattey, D. P., Atkinson, T. C., Barker, J. A., Fisher, R., Latin, J. P., Durrell, R., and Ainsworth, M.: Carbon dioxide, ground air and carbon cycling in Gibraltar karst, Geochimica Et Cosmochimica Acta, 184, 88-113, 2016.

Minami, M., Kato, T., Horikawa, K., and Nakamura, T.: Seasonal variations of 14C and δ13C for cave drip waters in Ryugashi Cave, Shizuoka Prefecture, central Japan, Nuclear Instruments and Methods in Physics Research Section B: Beam Interactions with Materials and Atoms, 362, 202-209, 2015.

Mook, W. G., Bommerson, J. C., and Staverman, W. H.: Carbon Isotope Fractionation between Dissolved Bicarbonate and Gaseous Carbon-Dioxide, Earth and Planetary Science Letters, 22, 169-176, 1974.

555   Moseley, G. E., Spotl, C., Brandstatter, S., Erhardt, T., Luetscher, M., and Edwards, R. L.: NALPS19: sub-
556   orbital-scale climate variability recorded in northern Alpine speleothems during the last glacial period,
557   Climate of the Past, 16, 29-50, 2020.
558   Nicolussi, K., Kaufmann, M., Patzelt, G., van der Plicht, J., and Thurner, A.: Holocene tree-line variability
559   in the Kauner Valley, Central Eastern Alps, indicated by dendrochronological analysis of living trees and
560   subfossil logs, Vegetation History and Archaeobotany, 14, 221-234, 2005.
561   Noronha, A. L., Johnson, K. R., Hu, C. Y., Ruan, J. Y., Southon, J. R., and Ferguson, J. E.: Assessing
562   influences on speleothem dead carbon variability over the Holocene: Implications for speleothem-
563   based radiocarbon calibration, Earth and Planetary Science Letters, 394, 20-29, 2014.
564   Noronha, A. L., Johnson, K. R., Southon, J. R., Hu, C. Y., Ruan, J. Y., and McCabe-Glynn, S.: Radiocarbon
565   evidence for decomposition of aged organic matter in the vadose zone as the main source of
566   speleothem carbon, Quaternary Science Reviews, 127, 37-47, 2015.
567   Polag, D., Scholz, D., Muhlinghaus, C., Spotl, C., Schroder-Ritzrau, A., Segl, M., and Mangini, A.: Stable
568   isotope fractionation in speleothems: Laboratory experiments, Chemical Geology, 279, 31-39, 2010.
569   Reimer, P. J., Bard, E., Bayliss, A., Beck, J. W., Blackwell, P. G., Ramsey, C. B., Buck, C. E., Cheng, H.,
570   Edwards, R. L., Friedrich, M., Grootes, P. M., Guilderson, T. P., Haflidason, H., Hajdas, I., Hatté, C.,
571   Heaton, T. J., Hoffmann, D. L., Hogg, A. G., Hughen, K. A., Kaiser, K. F., Kromer, B., Manning, S. W., Niu,
572   M., Reimer, R. W., Richards, D. A., Scott, E. M., Southon, J. R., Staff, R. A., Turney, C. S. M., and van der
573   Plicht, J.: IntCal13 and Marine13 Radiocarbon Age Calibration Curves 0–50,000 Years cal BP,
574   Radiocarbon, 55, 1869-1887, 2016.
575   Richards, D. A. and Dorale, J. A.: Uranium-series chronology and environmental applications of
576   speleothems, Uranium-Series Geochemistry, 52, 407-460, 2003.
577   Savitzky, A. and Golay, M. J. E.: Smoothing + Differentiation of Data by Simplified Least Squares
578   Procedures, Analytical Chemistry, 36, 1627-&, 1964.
579   Scholz, D. and Hoffmann, D.: ^{230}Th/U-dating of fossil reef corals and speleothems, Quater. Sci. J., 57,
580   52-77, 2008.
581   Scholz, D. and Hoffmann, D. L.: StalAge - An algorithm designed for construction of speleothem age
582   models, Quat. Geochronol., 6, 369-382, 2011.
583   Scholz, D., Mühlinghaus, C., and Mangini, A.: Modelling δ13C and δ18O in the solution layer on
584   stalagmite surfaces, Geochimica et Cosmochimica Acta, 73, 2592-2602, 2009.
585   Shi, Z., Allison, S. D., He, Y. J., Levine, P. A., Hoyt, A. M., Beem-Miller, J., Zhu, Q., Wieder, W. R.,
586   Trumbore, S., and Randerson, J. T.: The age distribution of global soil carbon inferred from radiocarbon
587   measurements, Nat. Geosci., 13, 555-+, 2020.
588   Southon, J., Noronha, A. L., Cheng, H., Edwards, R. L., and Wang, Y.: A high-resolution record of
589   atmospheric 14C based on Hulu Cave speleothem H82, Quaternary Science Reviews, 33, 32-41, 2012.
590   Spötl, C.: Long-term performance of the Gasbench isotope ratio mass spectrometry system for the
591   stable isotope analysis of carbonate microsamples, Rapid Communications in Mass Spectrometry, 25,
592   1683-1685, 2011.
593   Spotl, C., Fairchild, I. J., and Tooth, A. F.: Cave air control on dripwater geochemistry, Obir Caves
594   (Austria): Implications for speleothem deposition in dynamically ventilated caves, Geochimica Et
595   Cosmochimica Acta, 69, 2451-2468, 2005.
596   Spötl, C., Fohlmeister, J., Cheng, H., and Boch, R.: Modern aragonite formation at near-freezing
597   conditions in an alpine cave, Carnic Alps, Austria, Chemical Geology, 435, 60-70, 2016.
598   Spotl, C. and Mangini, A.: Speleothems and paleoglaciers, Earth and Planetary Science Letters, 254,
599   323-331, 2007.
600   Spötl, C. and Mangini, A.: Paleohydrology of a high-elecation, glacier influenced karst system in the
601   central alps (Austria), Austrian Journal of Earth Sciences, 103, 92-105, 2010.
602   Spötl, C., Mangini, A., Bums, S. J., Frank, N., and Pavuza, R.: Speleothems from the high-alpine
603   Spannagel cave, Zillertal Alps (Austria). In: Studies of cave sediments, Springer, 2004.
604   Spötl, C. and Mattey, D.: Stable isotope microsampling of speleothems for palaeoenvironmental
605   studies: A comparison of microdrill, micromill and laser ablation techniques, Chemical Geology, 235,
606   48-58, 2006.

607   Stuiver, M. and Polach, H. A.: Reporting of C-14 Data - Discussion, Radiocarbon, 19, 355-363, 1977.

608   Stuiver, M. and Robinson, S. W.: University of Washington GEOSECS north Atlantic carbon-14 results,
609   Earth and Planetary Science Letters, 23, 87-90, 1974.

610   Therre, S., Fohlmeister, J., Fleitmann, D., Matter, A., Burns, S. J., Arps, J., Schroder-Ritzrau, A., Friedrich,
611   R., and Frank, N.: Climate-induced speleothem radiocarbon variability on Socotra Island from the Last
612   Glacial Maximum to the Younger Dryas, Climate of the Past, 16, 409-421, 2020.

613   Tochterle, P., Dublyansky, Y., Stobener, N., Mandic, M., and Spotl, C.: High-resolution isotopic
614   monitoring of cave air CO2, Rapid Commun Mass Spectrom, 31, 895-900, 2017.

615   Trumbore, S.: Age of soil organic matter and soil respiration: Radiocarbon constraints on belowground
616   C dynamics, Ecological Applications, 10, 399-411, 2000.

617   Wackerbarth, A., Scholz, D., Fohlmeister, J., and Mangini, A.: Modelling the δ18O value of cave drip
618   water and speleothem calcite, Earth and Planetary Science Letters, 299, 387-397, 2010.

619   Welte, C., Wacker, L., Hattendorf, B., Christl, M., Fohlmeister, J., Breitenbach, S. F., Robinson, L. F.,
620   Andrews, A. H., Freiwald, A., and Farmer, J. R.: Laser Ablation–Accelerator Mass Spectrometry: An
621   Approach for Rapid Radiocarbon Analyses of Carbonate Archives at High Spatial Resolution, Analytical
622   chemistry, 88, 8570-8576, 2016a.

623   Welte, C., Wacker, L., Hattendorf, B., Christl, M., Koch, J., Synal, H. A., and Gunther, D.: Novel Laser
624   Ablation Sampling Device for the Rapid Radiocarbon Analysis of Carbonate Samples by Accelerator
625   Mass Spectrometry, Radiocarbon, 58, 419-435, 2016b.

626   Welte, C., Wacker, L., Hattendorf, B., Christl, M., Koch, J., Yeman, C., Breitenbach, S. F. M., Synal, H. A.,
627   and Gunther, D.: Optimizing the analyte introduction for C-14 laser ablation-AMS, Journal of Analytical
628   Atomic Spectrometry, 32, 1813-1819, 2017.

629   Yeman, C., Christl, M., Hattendorf, B., Wacker, L., Welte, C., Brehm, N., and Synal, H. A.: Unravelling
630   Quasi-Continuous 14C Profiles by Laser Ablation AMS, Radiocarbon, 62, 453-465, 2019.

631

632